NMR Structure of the Flavin Domain from Soluble Methane Monooxygenase Reductase from *Methylococcus capsulatus* (Bath)[†,‡]

Lisa L. Chatwood,[§] Jens Müller,[§,||,⊥] John D. Gross,[||] Gerhard Wagner,*[,||] and Stephen J. Lippard*[,§]

Department of Chemistry, Massachusetts Institute of Technology, Cambridge, Massachusetts 02139-4307, and Department of Biological Chemistry and Molecular Pharmacology, Harvard Medical School, Boston, Massachusetts 02115-5730

Received May 8, 2004; Revised Manuscript Received July 10, 2004

ABSTRACT: Soluble methane monooxygenase (sMMO) catalyzes the hydroxylation of methane by dioxygen to methanol, the first step in carbon assimilation by methanotrophs. This multicomponent system transfers electrons from NADH through a reductase component to the non-heme diiron center in the hydroxylase where O_2 is activated. The reductase component comprises three distinct domains, a [2Fe-2S] ferredoxin domain along with FAD- and NADH-binding domains. We report the solution structure of the reduced 27.6 kDa FAD- and NADH-binding domains (MMOR-FAD) of the reductase from *Methylococcus capsulatus* (Bath). The FAD-binding domain consists of a six-stranded antiparallel β-barrel and one α-helix, with the first 10 N-terminal residues unstructured. In the interface between the two domains, the FAD cofactor is tightly bound in an unprecedented extended conformation. The NADH-binding domain consists of a five-stranded parallel β-sheet with four α-helices packing closely around this sheet. MMOR-FAD is structurally homologous to other FAD-containing oxidoreductases, and we expect similar structures for the FAD/NADH-binding domains of reductases that occur in other multicomponent monooxygenases.

Methane monooxygenases (MMOs) are multicomponent enzyme systems with the extraordinary capability to oxidize the most inert of hydrocarbons, converting methane to methanol (*1*−*4*). They are expressed in methanotrophic bacteria, which use methane as their only source of energy and carbon. Since methanotrophs can oxidize a variety of other hydrocarbons and have been applied for bioremediation, they are of great chemical and biological as well as commercial interest (*5*, *6*).

The soluble methane monooxygenase (sMMO)[1] from *Methylococcus capsulatus* (Bath) consists of four components, a 251 kDa hydroxylase MMOH, a 15.9 kDa coupling protein MMOB, a 38.7 kDa reductase MMOR, and a 12 kDa protein of as yet unidentified function, MMOD (*7*−*9*). A full understanding of the mode of action of the enzyme requires the knowledge of the three-dimensional structures of its proteins. Investigations of the sMMO components from *M. capsulatus* (Bath) and other methanotrophs thus far have supplied X-ray crystal structures of MMOH (*10*−*14*) and NMR solution structures of MMOB (*15*, *16*) and the MMOR ferredoxin domain, MMOR-Fd, comprising 98 amino acids (*17*).

Because of the fairly large size of MMOR and the presence of a paramagnetic [2Fe-2S] cofactor, solving the NMR structure of the complete protein is challenging. We therefore decided to pursue this task with a three-step strategy. First, the structure of the reduced form of the smaller, paramagnetic MMOR-Fd was determined (*17*). In the present report we describe the solution structure of the reduced form of the second, 250 amino acid domain, MMOR-FAD. We chose to investigate the structure of the fully reduced protein because of its greater stability and the better comparability with the MMOR-Fd domain, which was solved previously in the reduced state. The entire MMOR structure will then be solved on the basis of these two individual building blocks. Crystal structures of similar proteins, including phthalate dioxygenase reductase (*18*) and benzoate-1,2-dioxygenase reductase (*19*), have already been solved, providing good comparisons for an NMR structure. Ultimately, knowledge of this reductase structure, together with the three-dimensional structure of MMOH, will enable us to interrogate long-range electron transfer reactions within and between soluble methane monooxygenase proteins.

MATERIALS AND METHODS

Expression of MMOR-FAD. An expression system for MMOR-FAD, the flavin domain of methane monooxygenase reductase, capable of growing on M9 minimal medium with high yields was produced by transforming the plasmid

[†] This work was supported by grants from the National Institute of General Medical Sciences (GM32134 to S.J.L., GM47467 and RR00995 to G.W.).

[‡] Structures have been deposited with the Brookhaven PDB database (PDB ID code: 1TVC). Chemical shifts have been deposited with the BioMagResBank (BMRB accession code 6295).

* Address correspondence to these authors. Tel: 617-253-1892. Fax: 617-258-8150. E-mail: gerhard_wagner@hms.harvard.edu (G.W.); lippard@mit.edu (S.J.L.).

[§] Massachusetts Institute of Technology.

[||] Harvard Medical School.

[⊥] Current address: Department of Chemistry, University of Dortmund, 44227 Dortmund, Germany.

[1] Abbreviations: BenC, benzoate 1,2-dioxygenase reductase; FAD, flavin adenine dinucleotide; FdR, NADPH:ferredoxin reductase; FlxR, flavodoxin reductase; FNR, ferredoxin-NADP$^+$ reductase; IPTG, isopropyl thio-β-galactose; MMOB, methane monooxygenase coupling protein; MMOH, methane monooxygenase hydroxylase; MMOR, methane monooxygenase reductase; MMOR-FAD, flavin- and NADH-binding domain of MMOR.; MMOR-Fd, ferredoxin domain of MMOR; NADH, nicotinamide adenine dinucleotide; OD, optical density; PDR, phthalate dioxygenase reductase; pMMO, particulate methane monooxygenase; sMMO, soluble methane monooxygenase.

10.1021/bi049066n CCC: $27.50
Published on Web 09/03/2004

pFAD21 into competent *Escherichia coli* BL21(DE3) cells. The plasmid was constructed by cutting the gene coding for MMOR-FAD out of pRED-FAD (*20*) and inserting it into the pET21(+) vector system (Novagen, Inc.), substituting a T7 promoter for the tac promoter present in pRED-FAD. The cells were grown in M9 minimal medium at 37 °C with constant shaking at 200 rpm. A concentration of 100 mg L^{-1} ampicillin was used for selection. When the OD_{600} value of the cell suspension reached 0.6 (or 0.4 for D_2O-based medium), expression was induced by adding IPTG to a final concentration of 0.1 mM. Cells were harvested after 12−15 h, and the protein was purified as described previously (*20*). The concentration of MMOR-FAD was determined by using an extinction coefficient of $\epsilon_{458} = 11300\ M^{-1}\ cm^{-1}$ (*20*). Because no FAD was added to any of the media, all of the cofactor incorporated into the protein had to be synthesized by the *E. coli* bacteria. As a consequence, the FAD moiety always showed the same isotopic labeling pattern as the corresponding protein.

^{15}N-Labeling of the protein was achieved by introducing 1 g L^{-1} of $^{15}NH_4Cl$ in the medium. For uniform ^{13}C-labeled protein, 2 g L^{-1} of ^{13}C glucose was used. Biosynthetic fractional ^{13}C labeling was performed with 10% ^{13}C glucose. Two samples of triple-labeled protein with different levels of deuteration were obtained by using $^{15}NH_4Cl$, ^{13}C glucose, and 70% and 99.9% D_2O, respectively. Perdeuterated MMOR-FAD samples with terminally ^{13}C,^{1}H methyl-labeled Ile, Leu, and Val residues were obtained by adding [3-^{13}C]-α-ketobutyrate and [3,3′-^{13}C]-α-ketoisovalerate to the medium, as described previously (*21*, *22*). In addition, 150 mg L^{-1} of natural abundance Phe, Tyr, and Trp were added at the same time as the ILV precursors to obtain ^{1}H labeling of aromatic side chains. Perdeuterated MMOR-FAD samples with protonated Tyr and Trp or Phe side chains were prepared by adding ^{15}N-labeled Phe or ^{15}N-labeled Tyr and unlabeled Trp to media containing $^{15}NH_4Cl$, 1,2,3,4,5,6,6-^{2}H−D-glucose and 99.9% D_2O. For selective ^{15}N amide labeling of Val, Phe, Tyr, and Leu residues, the plasmid pRED-FAD was transformed into competent *E. coli* DL39 cells, which are auxotrophs for Asp, Ile, Leu, Phe, Tyr, and Val. The resulting cells were grown in M9 minimal medium supplemented with 100 mg L^{-1} of each of the six amino acids, one of them with a ^{15}N-labeled amide group. Reverse selective labeling of Arg residues was achieved by growing BL21(DE3)/pRED-FAD cells in M9 minimal medium supplemented with 1 g L^{-1} of $^{15}NH_4Cl$ and 100 mg L^{-1} of natural abundance Arg. All isotopically labeled minimal media components and amino acids, with the exception of the ILV precursors, were purchased from Cambridge Isotope Laboratories.

NMR Experiments. NMR experiments were performed with reduced 0.6−1.0 mM MMOR-FAD in 50 mM sodium phosphate buffer, final pH of 6.7 after addition of $Na_2S_2O_4$, with 1 mM DTT, 0.1% NaN_3, and 2 mM Pefabloc (Roche Diagnostics GmbH, Germany). A final amount of 30 mM $Na_2S_2O_4$ and 3 equiv of NADH had to be added to keep the protein reduced. NMR tubes were filled under a nitrogen atmosphere and flame sealed.

Spectra were acquired at 750 MHz (Varian Unity Inova), 600 MHz (Bruker DRX), or 500 MHz (Bruker DRX equipped with a cryoprobe, or Varian Inova) at 25 °C unless stated otherwise. Backbone resonance assignments were obtained by using three-dimensional TROSY heteronuclear experiments (HNCA, HN(CO)CA, HN(CA)CB, HN(CO-CA)CB, HNCO, HN(CA)CO) and selective labeling techniques (*23*). Side chain assignments were obtained by using H(C-CO)NH-TOCSY, (H)C(CO)NH-TOCSY, ^{15}N TOCSY-HSQC, ^{15}N NOESY-HSQC, and ^{13}C NOESY-HSQC experiments (*23*). Stereospecific assignments of the methyl groups of 13 Leu and 10 Val residues were obtained with biosynthetic fractional ^{13}C labeling (*24*). Distance constraints were collected from ^{15}N NOESY-HSQC (100 ms mixing time at 25 °C and 60 ms mixing time at 35 °C), ^{13}C NOESY-HSQC (100 ms mixing time, fully ^{13}C-labeled protein), ^{13}C HMQC-NOESY (80 ms mixing time, ILV-methyl labeled protein with additionally ^{1}H-labeled (a) Tyr and Trp and (b) Phe residues), and homonuclear proton NOESY experiments (60 ms mixing time). Additional long-range distance constraints were gathered from ^{15}N-labeled, deuterated protein with protonated (a) Tyr and Trp or (b) Phe (180 ms, 25 °C) by ^{15}N NOESY-HSQC. Spectra were processed with FELIX (Molecular Simulations Inc., San Diego) or PROSA (*25*) and analyzed with XEASY (*26*) on Silicon Graphics work stations. The dihedral angle constraints for ϕ and ψ used in the calculations were obtained with the computer program TALOS (*27*).

Structure Calculations. NOESY cross-peaks were integrated by using the integration routine in the program DYANA (*28*). Interatomic upper-distance limits were calculated with the program CALIBA (*29*) based on NOESY cross-peak intensities for shorter mixing time experiments, or by collecting peak volumes into several bins and converting to distance by a factor of r^{-6} for experiments with long mixing times. Initial structure calculations were performed on Silicon Graphics workstations with the computer program DYANA (*28*) using simulated annealing by molecular dynamics in dihedral angle space. At all stages of the calculations, hydrogen bond constraints were introduced for residues determined to be in an α helix or a β strand. For each hydrogen bond two constraints were included into the calculations, $d_{NH\cdots O} = 1.8-2.4$ Å and $d_{N\cdots O} = 2.8-3.4$ Å. Methyl−methyl and methyl−aromatic constraints were added in later stage simulated annealing calculations performed in X-PLOR (*30*).

The FAD cofactor was incorporated into calculations by creating topology and parameter files in the program XPLO2D (*31*) from pdb coordinates of FAD in the crystal structure of the NADPH:ferredoxin reductase (FdR) from *Azotobacter vinelandii* (PDB code 1A8P) (*32*). Hydrogen atoms were added to FAD to result in the species $FADH_2$, which was optimized in InsightII (Accelrys, Inc.) prior to conversion in XPLO2D. The files were appended to earlier protein simulated annealing calculations for final structure calculation, and structures were viewed and statistics calculated using VMD (*33*). Protein figures were created with the program MOLMOL (*34*).

RESULTS

NMR Experiments. Backbone heavy atom and C^{β} resonances were assigned by using eight TROSY triple resonance experiments (HNCA/HN(CO)CA for 70% and 99% protein deuteration levels, HN(CA)CB/HN(COCA)CB and HNCO/HN(CA)CO) and ^{15}N selective labeling of valine, phenylalanine, tyrosine, and leucine, and reverse labeling of arginine residues as described previously (*23*, *35*). Resonances of 37

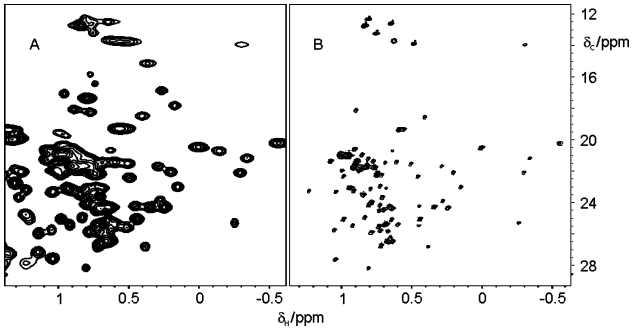

FIGURE 1: The aliphatic region of ^{13}C, ^{1}H HSQC spectra of MMOR-FAD for (A) uniformly ^{13}C-labeled MMOR-FAD (spectrum recorded on 500 MHz Bruker NMR spectrometer with cryoprobe for 1 mM protein sample) and (B) ^{13}C terminal methyl (ILV) labeled MMOR-FAD (0.6 mM protein sample, spectrum recorded on 600 MHz Bruker NMR spectrometer).

residues with extremely slowly exchanging amide protons were not detected in the triple resonance spectra of MMOR-FAD at the 99% deuteration level but could be assigned with an additional HNCA/HN(CO)CA pair when using protein with approximately 70% deuteration. These slow-exchanging protons were primarily found in the FAD-binding domain, including amide protons for amino acids 14−17, 27−32, 50−52, 54, 63−65, 69, 71, 73−79, 83, 85−88, 91−92, and 101−103. Residue 191 was the only amino acid of this type in the NADH-binding domain. Secondary structure elements were identified on the basis of ^{13}C chemical shift indices (*36*), dihedral angle constraints obtained from the program TALOS (*27*), and an analysis of NOE cross-peak patterns in the ^{15}N NOESY-HSQC and ^{13}C NOESY-HSQC spectra typical for α helices and β strands.

Significant improvement of peak resolution in the aliphatic region of the ^{13}C, ^{1}H spectra was observed for ILV-F and ILV-YW labeled proteins, as shown in Figure 1. This gain in resolution is obtained not only by limiting the total number of ^{13}C-labeled groups but also by providing spectra in which these protonated methyl groups are embedded in an otherwise perdeuterated background. A total of 247 methyl−methyl and methyl−aromatic constraints were collected from these experiments, greatly improving previously unstructured hydrophobic regions with few constraints. Additional long mixing time experiments on perdeuterated, ^{15}N-labeled protein with protonated Phe or Trp and Tyr side chains allowed assignment of aromatic protons and provided further long-range distance information. Several constraints between backbone amide protons and aromatic side chains to the N3 amide proton of the isoalloxazine moiety were also obtained to constrain the cofactor.

Solution Structure. For structure calculation, a total of 3653 constraints were used. Included are 1559 intraresidue constraints, 671 sequential, 239 medium-range, and 434 long-range NOE constraints, along with 247 methyl−methyl and methyl−aromatic NOE constraints from the spectra using ILV-labeled protein, 172 hydrogen-bond constraints, and 331 dihedral angle constraints. Of these constraints, 21 NOE, 90 dihedral, and two hydrogen-bond restraints were used to constrain the FAD cofactor within the protein structure. The core region of the protein, residues 10−250, has an average backbone rmsd of 0.98 Å for the set of 10 lowest energy structures. Average backbone rmsd values for secondary structures within individual domains, residues 10−111 for the FAD-binding domain and 113−245 for the NADH-binding domain, were 0.89 and 0.84, respectively. Structural statistics are summarized in Table 1. All calculated structures for MMOR-FAD converged, with the lowest energy structures containing no distance constraint violations greater than 0.5 Å or dihedral angle constraint violations greater than 5°.

Table 1: Statistics for the MMOR-FAD Solution Structure

NOE distance constraints	3150
intraresidue	1559
sequential ($\|i-j\|=1$)	671
medium range ($\|i-j\| \leq 4$)	239
$i, i+2$	92
$i, i+3$	100
$i, i+4$	47
long range ($\|i-j\| \geq 5$)	434
methyl constraints	247
H bond constraints	172
dihedral angle constraints[a]	331
average ensemble RMSD	
FAD domain (10−111)	0.89 Å
NADH domain (113−250)	0.84 Å
backbone (10−250)	0.98 Å
procheck analysis (%)	
most favored	90.2,[b] 67.2[c]
additional allowed	8.3,[b] 21.1[c]
generously allowed	1.0,[b] 8.7[c]
disallowed region	0.4,[b] 3.0[c]

[a] Dihedral angle constraints as obtained with TALOS (*27*) or generated using DYANA (*28*) based on NOE constraints. [b] Regular secondary structure. [c] Structured region (residues 10−251).

The NMR structure in Figure 2 reveals that MMOR-FAD consists of two domains, one containing the FAD cofactor and the other binding NADH. This structural feature is characteristic of proteins in the flavoprotein electron transferase family such as MMOR, phthalate dioxygenase reductase (PDR) (*18*), benzoate 1,2-dioxygenase reductase (BenC) (*19*), or NADPH:ferredoxin reductase (*32*). Figure 3A shows the sequence homology of MMOR-FAD to the flavin- and NAD(P)H-binding domains of these proteins. The FAD-binding domain of MMOR-FAD folds into a cylindrical six-stranded antiparallel β sheet and contains one α helix covering one opening of the cylinder. Many of the residues with slow-exchanging amide protons mentioned above are located within this β sheet, suggesting a rather rigid structure. The unstructured residues 2−10 are part of the linker between the Fd- and FAD-binding domains in the full-length protein. Residues 11−23 comprise strands Fβ1a and Fβ1b, which are broken by a loop region of residues 17−19 and are the first strand of the β-barrel. A tight loop back to strand Fβ2 (26−33) forms the next part of the sheet and is followed by a long, unstructured loop of residues 34−49. A short strand Fβ3 (50−53), loop, and Fβ4 (62−65) continue the cylinder sheet, followed by another, shorter unstructured loop of residues 66−75, parallel to the longer unstructured loop (34−49). Strand Fβ5 (76−80) leads into a loop of residues 81−88, followed by helix Fα1 (89−94) along one end of the β-barrel structure, which leads into Fβ6 (101−105), also part of the β sheet. Residues 106−120 form a coil linking the two domains. There is a cleft between strands Fβ4 and Fβ5, between which the isoalloxazine moiety and ribotyl chain of FAD bind. Direct evidence for flavin ring binding is seen in NMR spectra as discussed further below, and ribotyl chain binding is expected on the basis of sequence homology to other flavin-binding proteins.

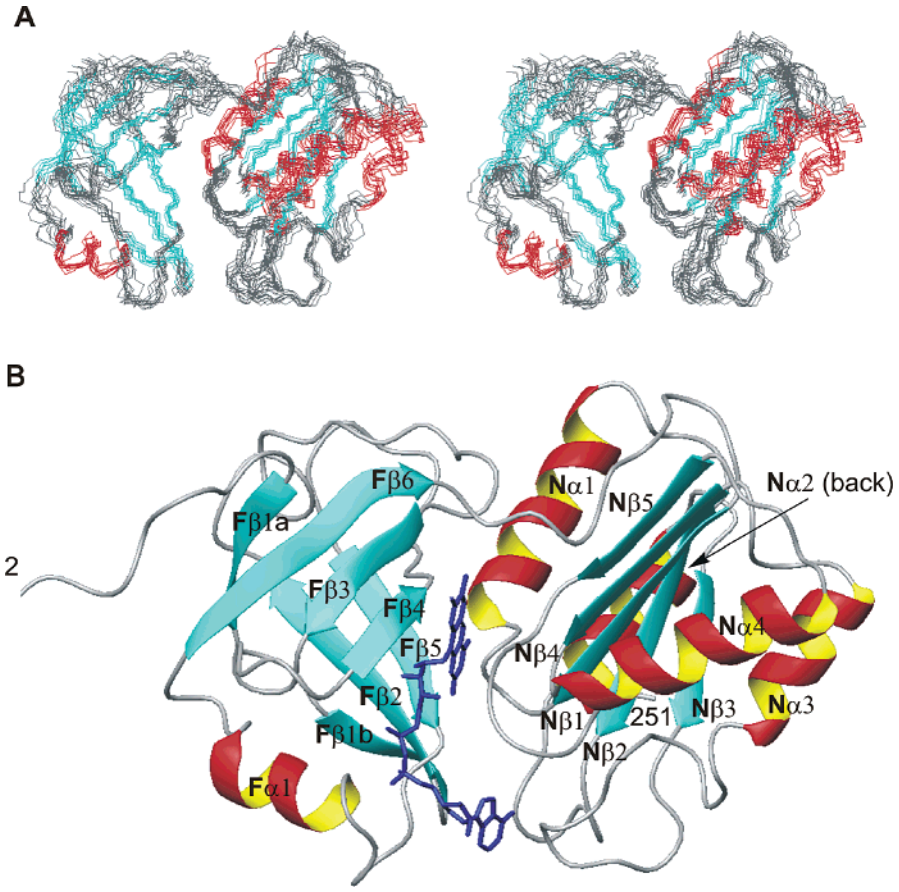

FIGURE 2: Solution structure of the FAD- and NADH-binding domains of MMOR. (A) The backbone atoms (N,Cα,C) of the 10 lowest energy NMR-derived structures are displayed in stereoview (residues 10−251). Secondary structural elements are shown colored in cyan (β sheet) and red (α helix). This figure was created by superimposing backbone atoms for residues 10−250 using MOLMOL (*34*). (B) Ribbon diagram and nomenclature of FAD- and NADH-domains, with bound FAD cofactor shown in blue at the interface between the two domains.

The NADH-binding domain contains alternating β strands and α helices forming a five-stranded parallel β sheet with two α helices positioned on each side of the sheet, thus resulting in a classical nucleotide binding fold. Residues 121−126 make up the central strand Nβ1 of this domain, followed by helix Nα1 comprising residues 130−143. After this helix, residues 144−148 loop leading into strand Nβ2 (149−154), next to Nβ1, followed by a long loop of residues 155−163 into helix Nα2 (164−173), then a short loop to strand Nβ3 (178−181) at the edge of the parallel β sheet. Another long loop leads to helix Nα3 with residues 199−207, followed by a loop to residues 213−217 in strand Nβ4 packed on the opposite side of strand Nβ1. A short loop leads into the long helix Nα4, with residues 220−233, which winds around in a long loop to strand Nβ5 (237−244). This final β strand sits next to Nβ4, finishing the β sheet with a strand order of Nβ3−Nβ2−Nβ1−Nβ4−Nβ5. The C-terminal tail loops back into the protein and rests between helices Nα2 and Nα3 and the β sheet.

FAD Cofactor Interactions. To constrain the FAD cofactor, a total of 21 FAD−protein and FAD−FAD NOEs were used, as well as one hydrogen bond, as shown in Figure 4. Both the C7 and C8 methyl groups on the flavin ring were observable in ^{13}C NOESY-HSQC spectra, and both the adenine-N6 amine and isoalloxazine-N3 amide protons were evident in ^{15}N NOESY-HSQC spectra. The ^{15}N chemical shifts of 147 ppm for N3 on the isoalloxazine ring and 79 ppm for AN6 on the adenine ring agree well with previously reported values of 145−154 ppm, for reduced flavins bound to proteins (*37*−*39*), and of 82−83 ppm, for free ^{15}N-labeled adenine, respectively (*40*). We were unable definitively to assign additional peaks to the FAD cofactor, due to the resolution of the collected spectra and peak crowding in regions expected for their chemical shifts. Assignment for the remaining nitrogen atoms in the FAD cofactor, as well as for the carbon and hydrogen atoms of the ribityl and ribotyl fragments, was ambiguous. The cross-peaks for FAD HN3 are given in Figure 5, along with corresponding backbone amide peaks for residues Ser65, Leu79, Arg81, and Leu246. The connecting lines denote several short contacts between the latter residues and those of the isoalloxazine group. The unusual upfield shift of the Leu246 amide proton suggests that it is stacking on top of the isoalloxazine ring. The amide peak for conserved Phe88 is shifted downfield to 12.04 ppm in the ^{1}H dimension, ∼2 ppm from other amide peaks in the spectrum. Furthermore, the magnitude of the peak in ^{15}N-labeled, perdeuterated protein exchanged into water is much smaller than average amide peaks, suggesting slow exchange. Together, these results provide evidence for a stable hydrogen bond involving the Phe88 amide proton. Since the ^{15}N NOESY-HSQC spectra did not reveal the identity of the corresponding hydrogen bond acceptor, and because in early structure calculations this amide proton was pointing toward the AMP phosphate of the FAD cofactor, two hydrogen bond constraints were added during later stages of the calculation.

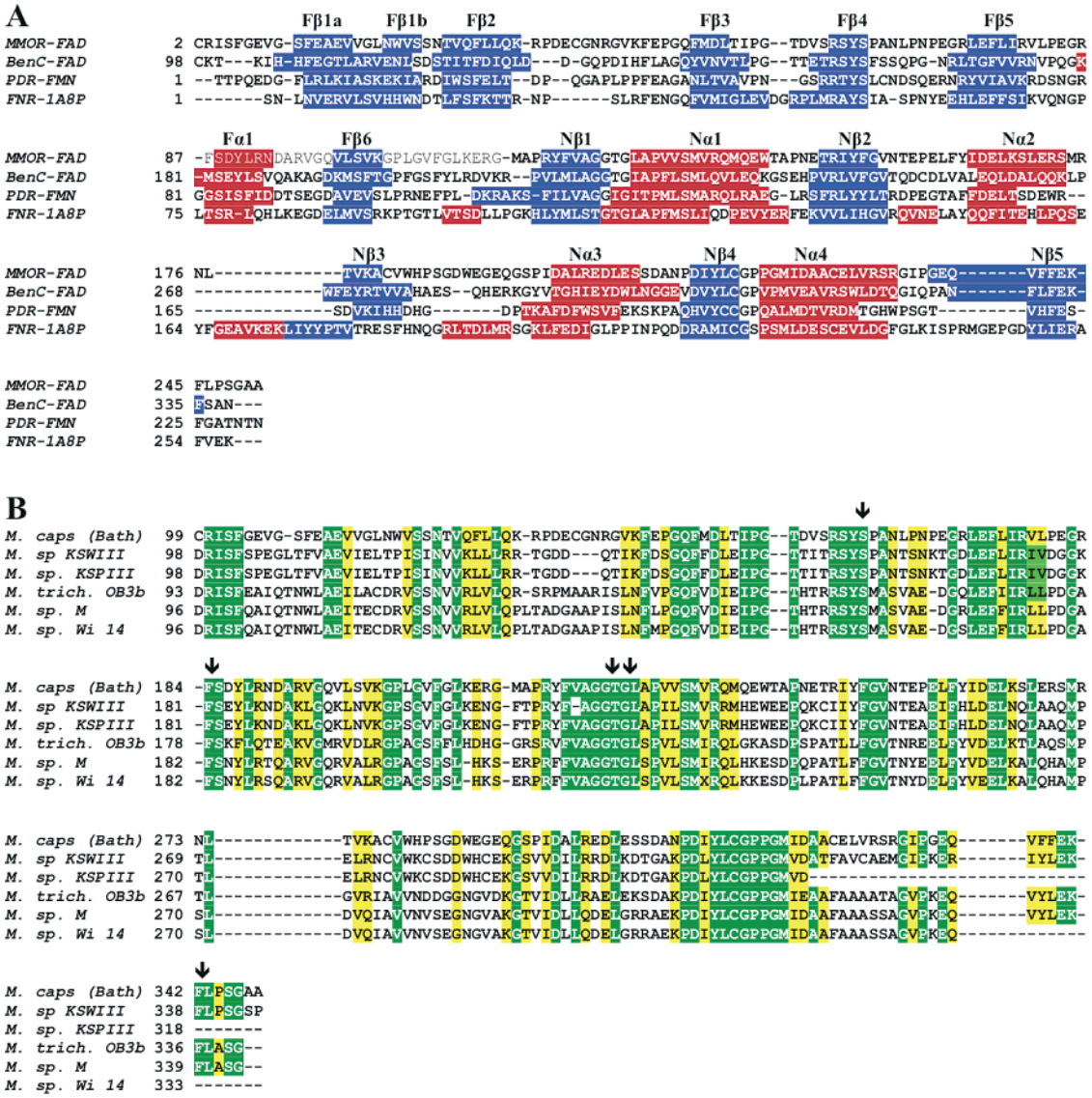

FIGURE 3: Sequence alignments of (A) FAD and NAD(P)H binding domain secondary structure of MMOR with benzoate-1,2-dioxygenase reductase (BenC, PDB code 1KRH) (*19*), phthalate dioxygenase reductase (PDR, PDB code 2PIA) (*18*), and NADPH:ferredoxin reductase (FdR, PDB code 1A8P) (*32*). Secondary structural elements are highlighted in red (α helices) or blue (*β* sheets). (B) Sequence alignments of the FAD- and NADH-binding domains of the reductases in soluble MMO from methanotrophs *M. capsulatus* (Bath) (*8*, *49*), *Methylomonas* sp. strains KSWIII and KSPIII (*50*), *Methylosinus trichosporium* OB3b (*51*, *52*), *Methylocystis* sp. strain M (*53*), and *Methylocystis* sp. strain Wi 14 (*54*). Identical residues are highlighted in dark green, whereas similar residues are in yellow. Residues marked with arrows are discussed in the text as being involved in FAD binding. Figures were made using BioEdit (*55*).

FAD is located at the interface between the domains (Figure 6) and converges in all structures with an rmsd value of 0.77 Å. The isoalloxazine moiety binds at the cleft between F*β*4 and F*β*5 in the FAD domain, with the C7M and C8M methyl groups protruding toward the linker between the two domains. The ribotyl chain extends along the cleft in the N-terminal domain *β* sheet, and the AMP phosphate group binds along the loop between F*β*5 and Fα1, its negative charge being compensated by an arginine side chain (Arg87). Amino acids Thr128/Gly129 and the C-terminal tail residues Phe245 and the amide proton of Leu246 lie near the *re*-face of the flavin ring. Experimental proof for this alignment can be found for example in the shielding of the Leu246 amide proton by the ring current effect of the flavin ring, resulting in an anomalous upfield shift (Figure 5). The N6 amine group of adenine is located along the loops between N*β*2 and Nα2 (residues 156−160) and N*β*3 and Nα3 (residues 187−189), creating an extended conformation of FAD with adenine binding along the edge of the domain interface away from the chain linking the domains. Figure 7 shows the FAD cofactor binding site and summarizes interactions between FAD and the protein.

DISCUSSION

MMOR-FAD Structure. MMOR has high sequence homology to other members of the flavoprotein electron transferase family. The FAD/NADH-binding domain of MMOR is structurally homologous to several other members of this class of proteins, most notably benzoate-1,2 dioxygenase reductase from *Acinetobacter* sp. strain ADP1 (*19*). Since BenC has an identical arrangement of ferredoxin-, FAD-, and NADH-binding domains, MMOR can be expected to have a similar structure. The structures for the FAD- and NADH-binding domains in both proteins are similar, with an rmsd value of 3.8 Å for superimposed structures. The major difference between these proteins occurs at the

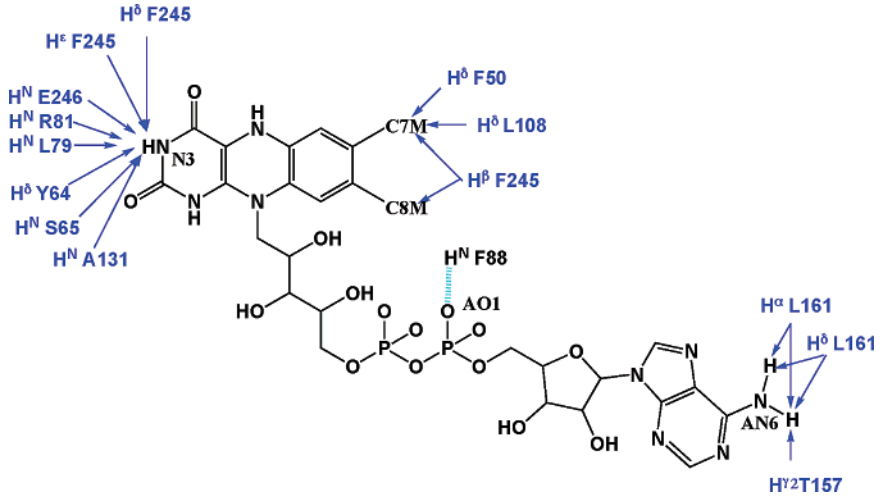

FIGURE 4: Intermolecular NOEs and hydrogen bonds between the protein and FAD cofactor. FAD is shown in black, with atom names listed, and blue arrows indicate intermolecular NOEs. The hydrogen bond between Phe88 and the phosphate oxygen AO1 is shown as a cyan dashed line.

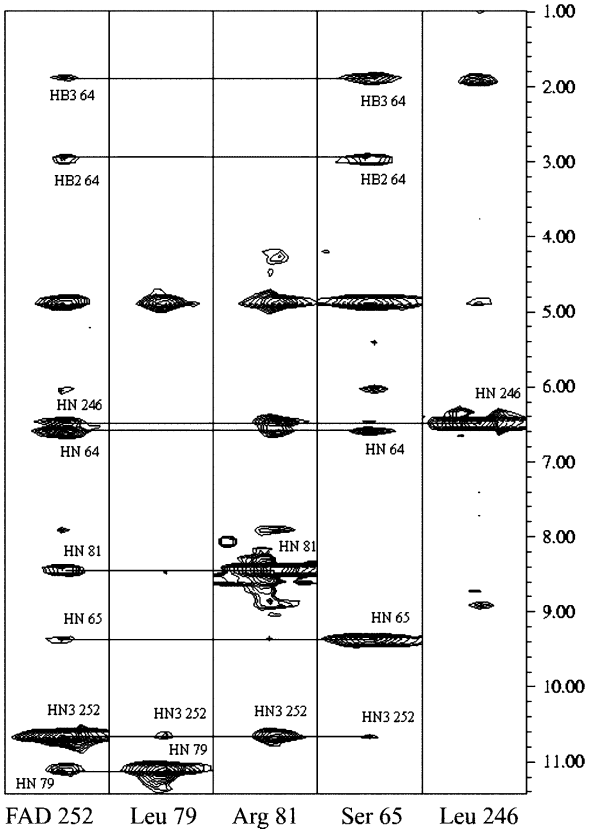

FIGURE 5: Selected strips from the 180 ms mixing time ^{15}N NOESY-HSQC spectrum with protonated Y and W residues in ^{15}N,^{2}H-labeled protein. FAD252 has a peak for HN3 in the first strip, with cross-peaks to $H^{\beta 2}$ and $H^{\beta 3}$ of Tyr64, HN of Ser65, HN of Leu79, HN of Arg81, and HN of Leu246. The corresponding strips show the amide peaks and their cross-peaks to FAD252. These interactions are direct evidence for FAD binding in MMOR-FAD.

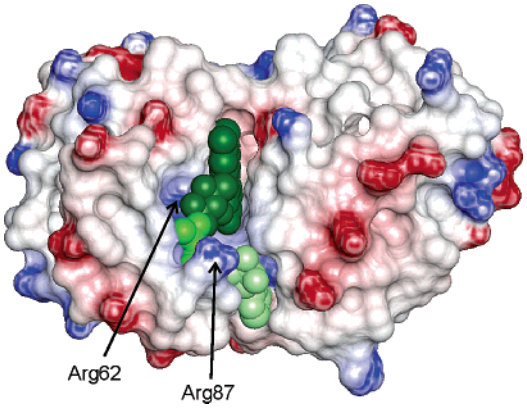

FIGURE 6: Electrostatic surface plot of the MMOR-FAD protein core (residues 11−251), revealing that the FAD cofactor is located in a cleft between the two domains. Red and blue represent negative and positive partial charges, respectively. The FAD prosthetic group is shown in green (dark green, riboflavin; green, phosphate groups; light green, adenosine). The positive charge provided by arginine side chains of the FAD-binding domain stabilizing the phosphate groups is clearly discernible. Figure 6 was generated with an algorithm (*56*) implemented in MolMol using relative dielectric constants of 3 and 80 for the protein and surrounding water, respectively. A box extending 10 Å away from the protein in each direction was used when calculating the potential.

C-terminus, where the MMOR tail folds back into the NADH-binding domain, whereas BenC has a tail extending to the surface of the protein.

The FAD-binding domain in MMOR is composed of an antiparallel β barrel with an α helix at one opening of the barrel. This domain is structurally homologous to other FAD-binding domains. Residues binding the FAD cofactor are strictly conserved within the reductase proteins of soluble MMO of methanotrophs, as shown in Figure 3B. The FAD itself is in an extended conformation so that the adenine moiety is distal from the isoalloxazine ring. This arrangement of the cofactor is unlike any conformation previously determined in the X-ray crystal structure analyses of homologous proteins (Figure 8D). Those structural studies resulted either in a bent conformation having the AMP moiety folding back toward the flavin ring or in an "extended" conformation where adenine is oriented away from it. In the bent conformation, the adenine group is held in place by hydrogen bonds involving its N6 and N7 nitrogen atoms and O3′ of the ribityl moiety (FdR, Figure 8C; BenC, Figure 8A) (*18*, *19*, *32*) with or without additional stabilization by stacking of an aromatic residue in the C-terminal region of the protein (Phe255 in FdR, Trp248 in flavodoxin reductase (FlxR) (*41*), no stacking in BenC). In the previously established "extended" conformation, no hydrogen bonding within the cofactor was observed. Instead, stacking on a

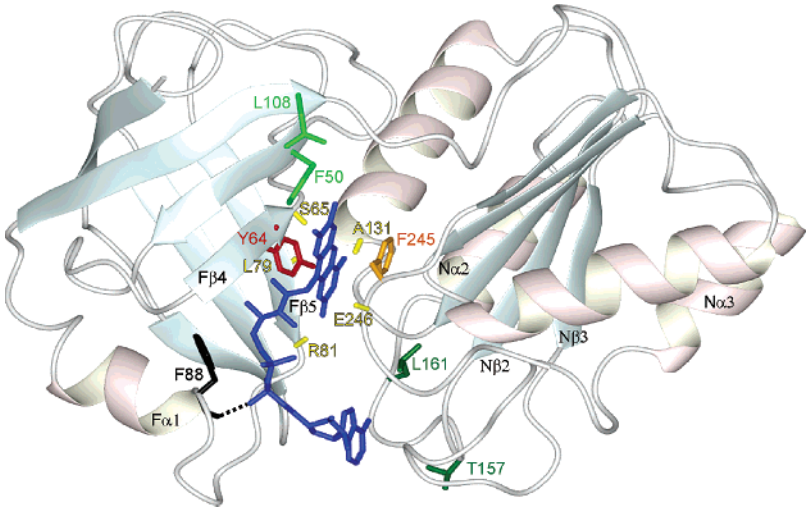

FIGURE 7: Experimentally observed contacts between FAD cofactor and protein. FAD is in blue, and the residues Phe245, Tyr64, and Phe88 as discussed in the text are shown in orange, red, and black, respectively. The hydrogen bond pointing from the Phe88 amide proton to the AMP phosphate group is also shown. Amino acids with observed contacts to the adenine-N6 group are in dark green, and those with contacts to the flavin methyl groups are in green. N−H bonds are displayed in yellow for residues with short contacts to the isoalloxazine N3 amide proton.

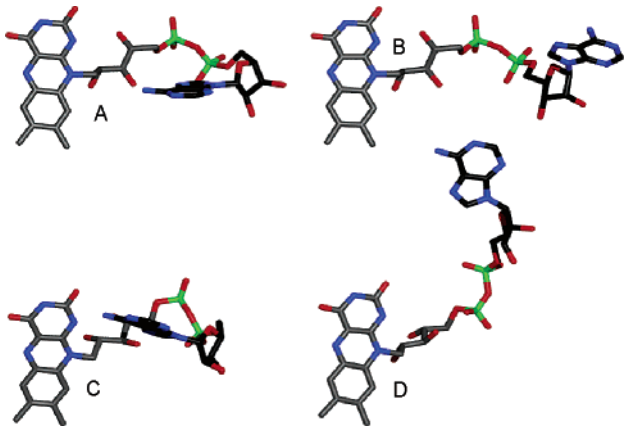

FIGURE 8: Comparison of the conformation of the FAD cofactor in different protein structures. A: BenC. B: spinach FNR. C: FdR. D: MMOR-FAD.

tyrosine side chain within an extended loop in the N-terminal domain preceding Fα1 was used for stabilization (Tyr120 in spinach ferredoxin-NADP$^+$ reductase (FNR), Figure 8B; Tyr104 in *Anabaena* FNR) (*42*−*44*). In the conformation found in MMOR-FAD, neither stacking on an aromatic side chain nor intraresidue hydrogen bonding is observed for the adenine moiety. Because of the presence of only a short loop between Fβ6 and Fα1, this behavior was predicted previously (*41*). The negative charge of the FAD phosphate groups is compensated by arginine side chains Arg62 and Arg87 (Figure 6), the first of which is strictly conserved within the sMMO family (Figure 3), and a hydrogen bond from the Phe88 amide group at the N-terminus of Fα1. Similar charge neutralization occurs in several other proteins of the flavodoxin reductase family (*32*, *41*, *43*). The isoalloxazine ring is in a very similar environment in all of the structures mentioned above, including MMOR-FAD. Nearly all structures display stacking of an aromatic residue from the C-terminal region of the protein (Phe245 in MMOR-FAD, none in FdR, Phe335 in BenC, Tyr247 in FlxR, Tyr314 in spinach FNR, Tyr303 in *Anabaena* FNR) on the *re*-face of the flavin ring, and all of them feature a nonperpendicular stacking interaction with a conserved tyrosine from the N-terminal domain on the *si*-face (Tyr64 in MMOR-FAD, Tyr53 in FdR, Tyr158 in BenC, Tyr52 in FlxR, Tyr95 in spinach FNR, Tyr79 in *Anabaena* FNR). The conserved tyrosine interaction with the *si*-face of the flavin ring has been proposed to be responsible for the correct positioning of the cofactor (*45*).

The loops at the end of the β barrel opposite to Fα1, residues 34−49 and 65−75, are less structured than the rest of the domain. In the crystal structures of PDR and BenC (*19*), the ferredoxin domain, which is missing in MMOR-FAD, is located in this region of the protein, suggesting that the disorder found here might arise from the absence of the ferredoxin domain in MMOR-FAD. The full-length structure of MMOR should resolve or further explain this discrepancy as well as that of the unusual FAD conformation. Additionally, the unstructured N-terminal chain should have a defined structure as a linker region between the ferredoxin- and FAD-binding domains.

NADH binding to MMOR-FAD could not be observed by NMR spectroscopy. No detectable signal of or cross-peaks to bound NADH, present in 3-fold excess in the solution, could be assigned in the NMR spectra. This result is not surprising considering that, in its reduced form, the protein has no requirement to bind additional NADH. On the basis of sequence homology to other FNR proteins crystallized with NAD(P)H analogues, NADH is expected to bind at the carboxy-terminal edge of Nβ1 and Nβ4 of the parallel β sheet (*19*, *43*). The conserved sequence GxGxxP (127−132), comprising the loop between Nβ1 and the N-terminus of Nα1, probably binds the diphosphate bridge in NADH (*46*). The adenine moiety is expected to be positioned between the N-terminus of Nα4 and the loop preceding Nα3 (*18*, *19*, *43*), facing away from the flavin-binding domain.

Structural Implications for Electron Transfer. Ferredoxin-NADP reductases are a remarkable family of proteins that can transfer electrons from ferredoxin to NAD(P)$^+$, or in the reverse direction through a bound flavin cofactor. The direction of electron transfer is determined by the redox potentials of the cofactors, which are modulated by the surrounding protein (*47*). Redox potentials of FAD in

MMOR are pH dependent (*20*, *48*), meaning that charged residues within MMOR modulate redox potential.

Phe245 (F342 in MMOR) is a conserved aromatic residue proposed in other proteins to act as a conformational gate regulating access of the nicotinamide moiety of NADH to the isoalloxazine ring (*19*). In the solution structure of the reduced protein, Phe245 is approximately 3.0 Å away from the *re*-face of FAD. Direct evidence for these interactions is observed in long mixing time (180 ms) $^{1}H,^{15}N$ NOESY spectra of perdeuterated, ^{15}N-labeled protein with protonated phenylalanine side chains. For the reduced form of MMOR, it is expected that this gate should block additional reduction by preventing binding of NADH, as well as stopping back electron transfer to oxidized NAD^+ by inducing its dissociation. Stopped flow experiments on both MMOR (*48*) and MMOR-FAD (*20*) give rate constants of 350 s^{-1} for a step after NADH binding prior to formation of a charge transfer complex between NADH and FAD. On the basis of our structure and the suggested role of Phe245 as a conformational gate, we propose that the gating movement of Phe245 and the concomitant displacement of the protein backbone are responsible for this observed rate constant for conversion of the initial Michaelis complex to the observed CT1 intermediate. In full-length MMOR, electron transfer from the FAD cofactor to the [2Fe-2S] cluster occurs with a rate constant of 90 s^{-1}, while NAD^+ simultaneously dissociates from MMOR (*48*). Kinetics data from MMOR-FAD alone measure this rate constant for dissociation to be 89 s^{-1} without electron transfer (*20*). Thus additional conformational changes in the protein as a result of NAD^+ dissociation appear to be responsible for regulating electron transfer.

CONCLUSIONS

We have solved the solution structure of the reduced FAD- and NADH-binding domains of MMOR by NMR spectroscopy. The results provide important structural information for the FAD- and NADH-binding domains in a reductase component of soluble MMO. On the basis of sequence homology, other sMMO reductases are expected to display similar protein folds. The structure of these domains is closely related to those available for other members of the FNR family, whereas the FAD cofactor is found in an unprecedented extended conformation. Information gathered from these results, together with the previously determined structure of MMOR-Fd (*17*), will facilitate solution of the full-length MMOR structure and ultimately allow a greater understanding of the mechanism of electron transfer within sMMO.

ACKNOWLEDGMENT

We thank G. Heffron for technical assistance and V. M. Gelev for synthesis of [3-^{13}C]-α-ketobutyrate and [3,3′-^{13}C]-α-ketoisovalerate. J.M. was a Feodor Lynen fellow of the Alexander von Humboldt Foundation (Germany). L.L.C. is the recipient of a predoctoral fellowship from the National Science Foundation.

REFERENCES

1. Merkx, M., Kopp, D. A., Sazinsky, M. H., Blazyk, J. L., Müller, J., and Lippard, S. J. (2001) Dioxygen activation and methane hydroxylation by soluble methane monooxygenase: A tale of two irons and three proteins, *Angew. Chem., Int. Ed. 40*, 2782−807.
2. Que, L., Jr., and Dong, Y. (1996) Modeling the oxygen activation chemistry of methane monooxygenase and ribonucleotide reductase, *Acc. Chem. Res. 29*, 190−6.
3. Liu, K. E., and Lippard, S. J. (1995) Studies of the soluble methane monooxygenase protein system: structure, component interactions and hydroxylation mechanism, *Adv. Inorg. Chem. 42*, 263−89.
4. Wallar, B. J., and Lipscomb, J. D. (1996) Dioxygen activation by enzymes containing binuclear non-heme iron clusters, *Chem. Rev. 96*, 2625−58.
5. Higgins, I. J., Best, D. J., and Hammond, R. C. (1980) New findings in methane-utilizing bacteria highlight their importance in the biosphere and their commercial potential, *Nature 286*, 561−4.
6. Fox, B. G., Borneman, J. G., Wackett, L. P., and Lipscomb, J. D. (1990) Haloalkene oxidation by the soluble methane monooxygenase from *Methylosinus trichosporium* OB3b: mechanistic and environmental implications, *Biochemistry 29*, 6419−27.
7. Colby, J., and Dalton, H. (1978) Resolution of the methane mono-oxygenase of *Methylococcus capsulatus* (Bath) into three components. Purification and properties of component C, a flavoprotein, *Biochem. J. 171*, 461−8.
8. Stainthorpe, A. C., Lees, V., Salmond, G. P., Dalton, H., and Murrell, J. C. (1990) The methane monooxygenase gene cluster of *Methylococcus capsulatus* (Bath), *Gene 91*, 27−34.
9. Merkx, M., and Lippard, S. J. (2002) Why OrfY? Characterization of MMOD, a long overlooked component of the soluble methane monooxygenase from *Methylococcus capsulatus* (Bath), *J. Biol. Chem. 277*, 5858−65.
10. Rosenzweig, A. C., Frederick, C. A., Lippard, S. J., and Nordlund, P. (1993) Crystal structure of a bacterial non-haem iron hydroxylase that catalyses the biological oxidation of methane, *Nature 366*, 537−43.
11. Rosenzweig, A. C., Brandstetter, H., Whittington, D. A., Nordlund, P., Lippard, S. J., and Frederick, C. A. (1997) Crystal structures of the methane monooxygenase hydroxylase from *Methylococcus capsulatus* (Bath): implications for substrate gating and component interactions, *Proteins 29*, 141−52.
12. Whittington, D. A., Rosenzweig, A. C., Frederick, C. A., and Lippard, S. J. (2001) Xenon and halogenated alkanes track putative substrate binding cavities in the soluble methane monooxygenase hydroxylase, *Biochemistry 40*, 3476−82.
13. Whittington, D. A., and Lippard, S. J. (2001) Crystal structures of the soluble methane monooxygenase hydroxylase from *Methylococcus capsulatus* (Bath) demonstrating geometrical variability at the dinuclear iron active site, *J. Am. Chem. Soc. 123*, 827−38.
14. Elango, N., Radhakrishnan, R., Froland, W. A., Wallar, B. J., Earhart, C. A., Lipscomb, J. D., and Ohlendorf, D. H. (1997) Crystal structure of the hydroxylase component of methane monooxygenase from *Methylosinus trichosporium* OB3b, *Protein Sci. 6*, 556−68.
15. Walters, K. J., Gassner, G. T., Lippard, S. J., and Wagner, G. (1999) Structure of the soluble methane monooxygenase regulatory protein B, *Proc. Natl. Acad. Sci. U.S.A. 96*, 7877−82.
16. Chang, S. L., Wallar, B. J., Lipscomb, J. D., and Mayo, K. H. (1999) Solution structure of component B from methane monooxygenase derived through heteronuclear NMR and molecular modeling, *Biochemistry 38*, 5799−812.
17. Müller, J., Lugovskoy, A. A., Wagner, G., and Lippard, S. J. (2002) NMR structure of the [2Fe-2S] ferredoxin domain from soluble methane monooxygenase reductase and interaction with its hydroxylase, *Biochemistry 41*, 42−51.
18. Correll, C. C., Batie, C. J., Ballou, D. P., and Ludwig, M. L. (1992) Phthalate dioxygenase reductase: a modular structure for electron transfer from pyridine nucleotides to [2Fe-2S], *Science 258*, 1604−10.
19. Karlsson, A., Beharry, Z. M., Eby, D. M., Coulter, E. D., Neidle, E. L., Kurtz, D. M., Jr., Eklund, H., and Ramaswamy, S. (2002) X-ray crystal structure of benzoate 1,2-dioxygenase reductase from *Acinetobacter* sp. strain ADP1, *J. Mol. Biol. 318*, 261−72.
20. Blazyk, J. L., and Lippard, S. J. (2002) Expression and characterization of ferredoxin and flavin adenine dinucleotide binding domains of the reductase component of soluble methane monooxygenase from *Methylococcus capsulatus* (Bath), *Biochemistry 41*, 15780−94.
21. Gross, J. D., Gelev, V. M., and Wagner, G. (2003) A sensitive and robust method for obtaining intermolecular NOEs between side chains in large protein complexes, *J. Biomol. NMR 25*, 235−42.

22. Hajduk, P. J., Augeri, D. J., Mack, J., Mendoza, R., Yang, J., Betz, S. F., and Fesik, S. W. (2000) NMR-based screening of proteins containing ^{13}C-labeled methyl groups, *J. Am. Chem. Soc. 122*, 7898−904.
23. Ferentz, A. E., and Wagner, G. (2000) NMR spectroscopy: a multifaceted approach to macromolecular structure, *Q. Rev. Biophys. 33*, 29−65.
24. Neri, D., Szyperski, T., Otting, G., Senn, H., and Wüthrich, K. (1989) Stereospecific nuclear magnetic resonance assignments of the methyl groups of valine and leucine in the DNA-binding domain of the 434 repressor by biosynthetically directed fractional ^{13}C labeling, *Biochemistry 28*, 7510−6.
25. Güntert, P., Dötsch, V., Wider, G., and Wüthrich, K. (1992) Processing of multidimensional NMR data with the new software PROSA, *J. Biomol. NMR 2*, 619−29.
26. Bartels, C., Xia, T.-H., Billeter, M., Güntert, P., and Wüthrich, K. (1995) The program XEASY for computer-supported NMR spectral analysis of biological macromolecules, *J. Biomol. NMR 6*, 1−10.
27. Cornilescu, G., Delaglio, F., and Bax, A. (1999) Protein backbone angle restraints from searching a database for chemical shift and sequence homology, *J. Biomol. NMR 13*, 289−302.
28. Güntert, P., Mumenthaler, C., and Wüthrich, K. (1997) Torsion angle dynamics for NMR structure calculation with the new program DYANA, *J. Mol. Biol. 273*, 283−98.
29. Güntert, P., Braun, W., and Wüthrich, K. (1991) Efficient computation of three-dimensional protein structures in solution from nuclear magnetic resonance data using the program DIANA and the supporting programs CALIBA, HABAS and GLOMSA, *J. Mol. Biol. 217*, 517−30.
30. Brünger, A. T. (1992) *X-PLOR manual 3.1: A system for X-ray crystallography and NMR*, Yale University Press, New Haven, CT.
31. Kleywegt, J. T. (1995) Dictionaries for heteros, *CCP/ESF-EACBM Newsl. Protein Crystallogr. 31*, 45−50.
32. Sridhar Prasad, G., Kresge, N., Muhlberg, A. B., Shaw, A., Jung, Y. S., Burgess, B. K., and Stout, C. D. (1998) The crystal structure of NADPH:ferredoxin reductase from *Azotobacter vinelandii*, *Protein Sci. 7*, 2541−9.
33. Humphrey, W., Dalke, A., and Schulten, K. (1996) VMD: Visual Molecular Dynamics, *J. Mol. Graphics 14*, 33−8.
34. Koradi, R., Billeter, M., and Wüthrich, K. (1996) MOLMOL: a program for display and analysis of macromolecular structures, *J. Mol. Graphics 14*, 51−5.
35. Chou, J. J., Matsuo, H., Duan, H., and Wagner, G. (1998) Solution structure of the RAIDD CARD and model for CARD/CARD interaction in caspase-2 and caspase-9 recruitment, *Cell 94*, 171−80.
36. Wishart, D. S., and Sykes, B. D. (1994) The ^{13}C chemical-shift index: a simple method for the identification of protein secondary structure using ^{13}C chemical-shift data, *J. Biomol. NMR 4*, 171−80.
37. Fleischmann, G., Lederer, F., Müller, F., Bacher, A., and Rüterjans, H. (2000) Flavin-protein interactions in flavocytochrome b2 as studied by NMR after reconstitution of the enzyme with ^{13}C- and ^{15}N-labelled flavin, *Eur. J. Biochem. 267*, 5156−67.
38. Griffin, K. J., Degala, G. D., Eisenreich, W., Müller, F., Bacher, A., and Frerman, F. E. (1998) ^{31}P-NMR spectroscopy of human and *Paracoccus denitrificans* electron transfer flavoproteins, and ^{13}C- and ^{15}N-NMR spectroscopy of human electron transfer flavoprotein in the oxidised and reduced states, *Eur. J. Biochem. 255*, 125−32.
39. Rüterjans, H., Fleischmann, G., Knauf, M., Löhr, F., Blümel, M., Lederer, F., Mayhew, S. G., and Müller, F. (1996) NMR studies of flavoproteins, *Biochem. Soc. Trans. 24*, 116−21.
40. Shallop, A. J., Gaffney, B. L., and Jones, R. A. (2003) Use of ^{13}C as an indirect tag in ^{15}N specifically labeled nucleosides. Syntheses of [8-^{13}C-1,7,NH_2-$^{15}N_3$]adenosine, -guanosine, and their deoxy analogues, *J. Org. Chem. 68*, 8657−61.
41. Ingelman, M., Bianchi, V., and Eklund, H. (1997) The three-dimensional structure of flavodoxin reductase from *Escherichia coli* at 1.7 Å resolution, *J. Mol. Biol. 268*, 147−57.
42. Bruns, C. M., and Karplus, P. A. (1995) Refined crystal structure of spinach ferredoxin reductase at 1.7 Å resolution: oxidized, reduced and 2′-phospho-5′-AMP bound states, *J. Mol. Biol. 247*, 125−45.
43. Karplus, P. A., Daniels, M. J., and Herriott, J. R. (1991) Atomic structure of ferredoxin-NADP$^+$ reductase: prototype for a structurally novel flavoenzyme family, *Science 251*, 60−6.
44. Serre, L., Vellieux, F. M. D., Medina, M., Gómez-Moreno, C., Fontecilla-Camps, J. C., and Frey, M. (1996) X-ray structure of the ferredoxin:NADP$^+$ reductase from the cyanobacterium *Anabaena* PCC 7119 at 1.8 Å resolution, and crystallographic studies of NADP$^+$ binding at 2.25 Å resolution, *J. Mol. Biol. 263*, 20−39.
45. Arakaki, A. K., Orellano, E. G., Calcaterra, N. B., Ottado, J., and Ceccarelli, E. A. (2001) Involvement of the flavin *si*-face tyrosine on the structure and function of ferredoxin-NADP$^+$ reductases, *J. Biol. Chem. 276*, 44419−26.
46. Correll, C. C., Ludwig, M. L., Bruns, C. M., and Karplus, P. A. (1993) Structural prototypes for an extended family of flavoprotein reductases: comparison of phthalate dioxygenase reductase with ferredoxin reductase and ferredoxin, *Protein Sci. 2*, 2112−33.
47. Carrillo, N., and Ceccarelli, E. A. (2003) Open questions in ferredoxin-NADP$^+$ reductase catalytic mechanism, *Eur. J. Biochem. 270*, 1900−15.
48. Kopp, D. A., Gassner, G. T., Blazyk, J. L., and Lippard, S. J. (2001) Electron-transfer reactions of the reductase component of soluble methane monooxygenase from *Methylococcus capsulatus* (Bath), *Biochemistry 40*, 14932−41.
49. Coufal, D. E., Blazyk, J. L., Whittington, D. A., Wu, W. W., Rosenzweig, A. C., and Lippard, S. J. (2000) Sequencing and analysis of the *Methylococcus capsulatus* (Bath) soluble methane monooxygenase genes, *Eur. J. Biochem. 267*, 2174−85.
50. Shigematsu, T., Hanada, S., Eguchi, M., Kamagata, Y., Kanagawa, T., and Kurane, R. (1999) Soluble methane monooxygenase gene clusters from trichloroethylene-degrading *Methylomonas* sp. strains and detection of methanotrophs during in situ bioremediation, *Appl. Environ. Microbiol. 65*, 5198−206.
51. Fox, B. G., Liu, Y., Dege, J. E., and Lipscomb, J. D. (1991) Complex formation between the protein components of methane monooxygenase from *Methylosinus trichosporium OB3b*. Identification of sites of component interaction, *J. Biol. Chem. 266*, 540−50.
52. Cardy, D. L. N., Laidler, V., Salmond, G. P., and Murrell, J. C. (1991) The methane monooxygenase gene cluster of *Methylosinus trichosporium*: cloning and sequencing of the mmoC gene, *Arch. Microbiol. 156*, 477−83.
53. McDonald, I. R., Uchiyama, H., Kambe, S., Yagi, O., and Murrell, J. C. (1997) The soluble methane monooxygenase gene cluster of the trichloroethylene-degrading methanotroph *Methylocystis* sp. strain M, *Appl. Environ. Microbiol. 63*, 1898−904.
54. Grosse, S., Laramee, L., Wendlandt, K. D., McDonald, I. R., Miguez, C. B., and Kleber, H. P. (1999) Purification and characterization of the soluble methane monooxygenase of the type II methanotrophic bacterium *Methylocystis* sp. strain WI 14, *Appl. Environ. Microbiol. 65*, 3929−35.
55. Hall, T. A. (1999) BioEdit: a user-friendly biological sequence alignment editor and analysis program for Windows 95/98/NT, *Nucleic Acids Symp. Ser. 41*, 95−8.
56. Nicholls, A., and Honig, B. (1991) A rapid finite difference algorithm, utilizing successive over-relaxation to solve the Poisson−Boltzmann equation, *J. Comput. Chem. 12*, 435−445.

BI049066N